Biochemical and Biophysical Research Communications 453 (2014) 636–641

Contents lists available at ScienceDirect

Biochemical and Biophysical Research Communications

journal homepage: www.elsevier.com/locate/ybbrc

Revelation of endogenously bound Fe^{2+} ions in the crystal structure of ferritin from *Escherichia coli*

Viswanathan Thiruselvam [a], Padavattan Sivaraman [b], Thirumananseri Kumarevel [b,c,*], Mondikalipudur Nanjappagounder Ponnuswamy [a,*]

[a] Centre of Advanced Study in Crystallography and Biophysics, University of Madras, Guindy Campus, Chennai 600 025, India
[b] RIKEN SPring-8 Center, Harima Institute, 1-1-1 Kouto, Sayo, Hyogo 679-5148, Japan
[c] Structural Biology Laboratory, RIKEN Yokohama Institute, RIKEN, 1-7-22 Suehiro-cho, Tsurumi, Yokohama 230-0045, Japan

ARTICLE INFO

Article history:
Received 26 September 2014
Available online 12 October 2014

Keywords:
Ferritin
Iron regulation
Binuclear iron site

ABSTRACT

Ferritin is an iron regulatory protein. It is responsible for storage and detoxification of excess iron thereby it regulates iron level in the body. Here we report the crystal structure of ferritin with two endogenously expressed Fe atoms binding in both the sites. The protein was purified and characterized by MALDI-TOF and N-terminal amino acid sequencing. The crystal belongs to I4 space group and it diffracted up to 2.5 Å. The structural analysis suggested that it crystallizes as hexamer and confirmed that it happened to be the first report of endogenously expressed Fe ions incorporated in both the A and B sites, situated in between the helices.

© 2014 Elsevier Inc. All rights reserved.

1. Introduction

Iron is an important element, and it performs many cellular functions such as cell growth, oxygen transport, electron transfer, nitrogen fixation, DNA synthesis, and also involved in the synthesis of hemoglobin and myoglobin proteins [1]. On the other hand, excess of iron leads to the formation of harmful free radicals such as hydroperoxyl radical ($HOO^{\cdot}$), and hydroxyl radical ($HO^{\cdot}$), which increases the toxicity level and can be interpreted through Fenton reaction,

$$Fe^{2+} + H_2O_2 + H^+ \rightarrow Fe^{3+} + HO^{\cdot} + H_2O$$
$$Fe^{3+} + H_2O_2 \rightarrow Fe^{2+} + HOO^{\cdot} + H^+$$

Ferritins are the super family proteins and capable of accepting, storing and donating the iron when the requirement arises. The family can be classified into three sub-families, namely the iron storing ferritin (Ftn), heme containing bacterio ferritin (Bfr) and DNA-binding protein from starved cells (Dps) [2–7]. Ferritin also involves in many biochemical pathways, which regulates cell proliferation, apoptosis, and protein translation.

The architecture of ferritin protein is in the form of a hollow shell with 12 and 8 nm inner and outer diameter. It consists of 24 subunits and about 4500 iron atoms stored in the centre of the cavity [8,9]. The exterior and interior shells are connected by channels along 2, 3 and 4-fold symmetry axes [10]. Both the hydrophilic and hydrophobic pores in ferritin are responsible for the entry of iron atoms and stability.

Ferritin protein is also classified as heavy (H) and light (L) chain subunits. Both the subunits are about 55% sequence similarity and regulate the functions differently. The heavy chain (H) with the molecular weight of 24 kDa involved in the enzymatic activity; oxidize Fe (II) to Fe (III) states. The presence of ferroxidase centre in heavy chain (H) ferritin plays a vital role in iron uptake, due to the overcrowding of glutamic acid residues. The mutations of Glu62 and His65 lead to the lack of iron uptake and confirmed in human and mouse ferritins [11,12]. Light chain (L) with a molecular weight of 19 kDa cannot perform the above said activities due to the presence of a number of carboxyl groups. The L chain acts as an iron nucleation site and capable of mineralizing iron faster than the heavy chain (H) of ferritin. L ferritin stands out to be higher stability than H ferritin even under acidic and reducing conditions [13,14].

The platinum based anticancer drugs are the main source for tumors; however the toxicity increases due to the excess usage of platinum based drugs. Afterwards the bigger molecules with large cavity are used as a vehicle for drug transport (Cucurbituril series) but failure was unavoidable due to their lower water solubility. Recent studies showed that, macromolecules of large cavity along with higher solubility of protein (ferritin) were

* Corresponding authors at: Structural Biology Laboratory, RIKEN Yokohama Institute, RIKEN, 1-7-22 Suehiro-cho, Tsurumi, Yokohama 230-0045, Japan. Fax: +81 45 503 9480 (T. Kumarevel). Fax: +91 44 2230 0122 (M.N. Ponnuswamy).
E-mail addresses: kumarevel.thirumananseri@riken.jp (T. Kumarevel), mnpsy2004@yahoo.com, mnpsy2004@hotmail.com (M.N. Ponnuswamy).

http://dx.doi.org/10.1016/j.bbrc.2014.10.007
0006-291X/© 2014 Elsevier Inc. All rights reserved.

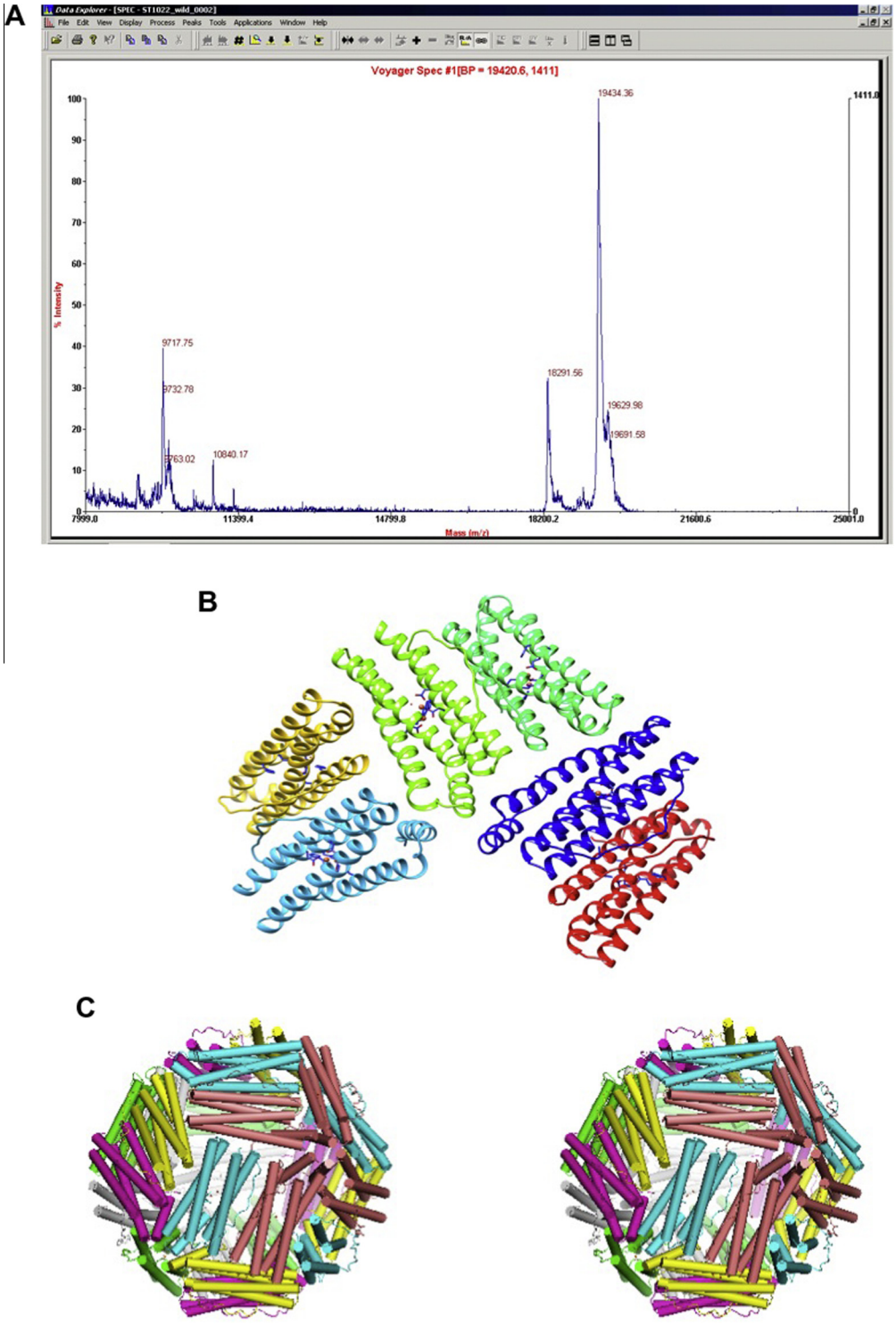

Fig. 1. Characterization and structural representation of *E. coli* ferritin. (A) MALDI-TOP spectrum of purified protein, (B) hexameric structure of crystallized ferritin in the asymmetric unit shown as cartoon representations, the active site residues are shown by ball-and-stick model and Fe-ions by spheres, (C) biological assembly of ferritin molecules (24-mer) are show in stereo view. The helices are represented by cylindrical and the bound metal ions are shown by spheres.

used as best drug delivery system. The ferritin molecules in the inner core are capable of adhesive of metal and nano particles. Anticancer drugs such as Cisplatin and Carboplatin are incorporated into ferritin molecules based on pH values using refolding mechanism. The binding capability of anti-cancer drugs in ferritin is used as ligand-receptor mediated drug delivery systems [15,16].

2. Materials and methods

2.1. Purification

The *Nde*I and *Bam*HI digested PCR product cloned into pET-21a(+) vector (Novagen). The cloned plasmid was transformed into *Escherichia coli* BL21-CodonPlus (DE3)-RIL-X strain. The

Table 1
Data collection and refinement statistics of ferritin.

Crystal parameters	Ferritin crystal
Data collection	
Space group	I4
Unit cell	a = 127.998; b = 127.998; c = 170.902
No. of molecules in ASU	6
Solvent content	59.17
Resolution range (Å)	50.0–2.50 (2.54–2.50)
Total reflections	1,356,049
Unique reflections	47,454 (4739)
Completeness	99.98 (100)
Redundancy	3.7 (3.9)
R_{merge}[a]	0.092 (0.608)
Refinement	
Resolution range (Å)	35.31–2.50
R_{work}[b]	0.1719
R_{free}[c]	0.2354
Number of protein atoms	8148
Number of Fe^{2+} ions	12
Number of SO_4 ions	19
Number of Hg ions	2
Number of Cl_2 ions	27
Number of Mg^{2+} ions	1
Number of MES molecules	1
Number of water molecules	197
R_{msd} bond lengths (Å)	0.0134
R_{msd} bond angles (°)	1.5228
Average B-factor (Å^2)	48.10
Ramachandran statistics	
Most favored region (%)	97.02
Allowed region (%)	2.16
PDB ID	4REU

[a] $R_{merge} = \Sigma h\ \Sigma i|I(h,i) - \langle I(h)\rangle|/\Sigma h\ \Sigma i\ I(h,i)$, where $I(h,i)$ is the intensity value of the ith measurement of h and $\langle I(h)\rangle$ is the corresponding mean value of $I(h)$ for all i measurements.

[b] $R_{factor} = \Sigma||F_{obs}| - |F_{calc}||/|F_{obs}|$, where $|F_{obs}|$ and $|F_{calc}|$ are the observed and calculated structure factor amplitudes, respectively.

[c] R_{free} is the same as R factor, but for a 5% subset of all reflections.

protein was over expressed at mid-log phase by addition of 1 mM IPTG. Cells were harvested by centrifugation, and suspended in buffer containing 20 mM Tris–HCl pH 8.0, 50 mM NaCl, 5 mM β-mercaptoethanol and sonicated. The total lysate was incubated with DNase I and RNase A with 5 mM of $CaCl_2$ and 25 mM of $MgCl_2$ for 30 min. The soluble proteins in the supernatant solution was precipitated by adding 80% of the ammonium sulfate and centrifuged at high speed (15,000 rpm) and removed the supernatant solution. The protein-containing pellet was dialyzed against the buffer solution (20 mM Tris–HCl pH 8.0, 50 mM NaCl) and further purified by hydrophobic columns (Resource ISO, Resource PHE1, GE Healthcare Biosciences) using ammonium sulfate gradient method. Finally the sample was concentrated and applied into gel filtration column (Superdex 75, GE Healthcare Biosciences). The purity of the sample was analyzed in SDS–PAGE.

2.2. MALDI-TOF mass spectroscopy analysis

The molecular weight and purity of ferritin were analyzed by a matrix-assisted laser desorption/ionization time-of-flight (MALDI-TOF) mass spectrometer using Voyager-DE pro (Applied Bio System). 1 mg of sinapic acid was dissolved in 25 μL of milliQ water, 25 μL of acetonitrile were added and 0.4 μL of trifluro acidic acid was mixed with above mixture and homogenated thoroughly using table-top centrifuge. The protein sample mixed with the above said mixture in 1:1 ratio and loaded in the sample tray. The spectrum results were shown in Fig. 1A.

2.3. N-terminal protein sequencing

N-terminal protein sequencing was performed by Edman degradation method, using PROCISE protein sequencer for the purified protein sample. 10 μL methanol was added to membrane to bring to wet condition. 100 μL of protein sample (1 pmol/μL) was added to membrane and loaded. The 20 amino acids in the N-terminal region was identified and given as follows**: M L K P E M I E K L N E Q M N L E L Y S.**

2.4. Crystallization and data collection

Purified protein sample was concentrated up to 12 mg/ml and used for crystallization purpose. Initial crystallization trails were performed by hanging drop vapor diffusion and batch methods using Hampton Crystal Screen, Crystal Screen II, wizard crystallization kit I, II and Hampton Natrix kit I and II. Better diffracting quality crystals were obtained in 10 mM $MgCl_2$ hexahydrate, 0.05 M MES pH 5.6, 2 M Lithium sulfate condition. Suitable crystals were mounted and collected the diffraction data on RIKEN Structural Genomics Beam line II (BL26B2) at SPring-8 Center, Hyogo, Japan. All crystal data were processed with the *HKL*-2000 program suite.

2.5. Structure refinement

The ferritin molecule crystallized in I4 space group and the Matthews coefficient analysis showed that there are six molecules in the asymmetric unit with the solvent content of 59.17% [17]. The structure solution and refinement were performed by molecular replacement method with 1EUM as a search model using CCP4 suite [18]. Model applied to 10 cycles of rigid body followed by restrained Refmac refinement. Further model building was carried out using coot program [19].

3. Results

The *E. coli* ferritin was expressed and purified using different types of chromatographic methods. The purified sample was confirmed through MALDI-TOF MS, the single peak was observed at m/z 19418.418.

The protein sequencer identified 20 amino acids in N-terminal region as follows, **M L K P E M I E K L N E Q M N L E L Y S**. We crystallized the protein using hanging drop vapor diffusion method. The crystal data were collected in synchrotron source and solved by MR method.

3.1. Overall structure

Ferritin crystallizes in I4 space group and consists of three dimers related by a non-crystallographic 3-fold axis in the asymmetric unit. Each subunit is composed of 165 amino acids. The structure of each monomer is arranged as H-H-L-H-H-L-H (four α helix, followed by a fifth α helix through 18 and 6 residue loops). While refining the structure, the unambiguous electron density showed the Fe binding region. The overall electron density map revealed 12 Fe atoms, 2 $HgCl_2$ molecules, 19 SO_4 ions, 27 Cl ions, one Mg^{2+}, one MES and 197 water molecules in the asymmetric unit (Fig. 1B). The biological assembly of ferritin composed of 24 subunits, which is four hexamers (3-dimers) of ferritin related by a crystallographic 4-fold axis (Fig. 1C). The molecules were refined to an acceptable stereochemistry and final R factor stands out to be 0.17 (R_{free} 0.23) at 2.5 Å resolution (Table 1).

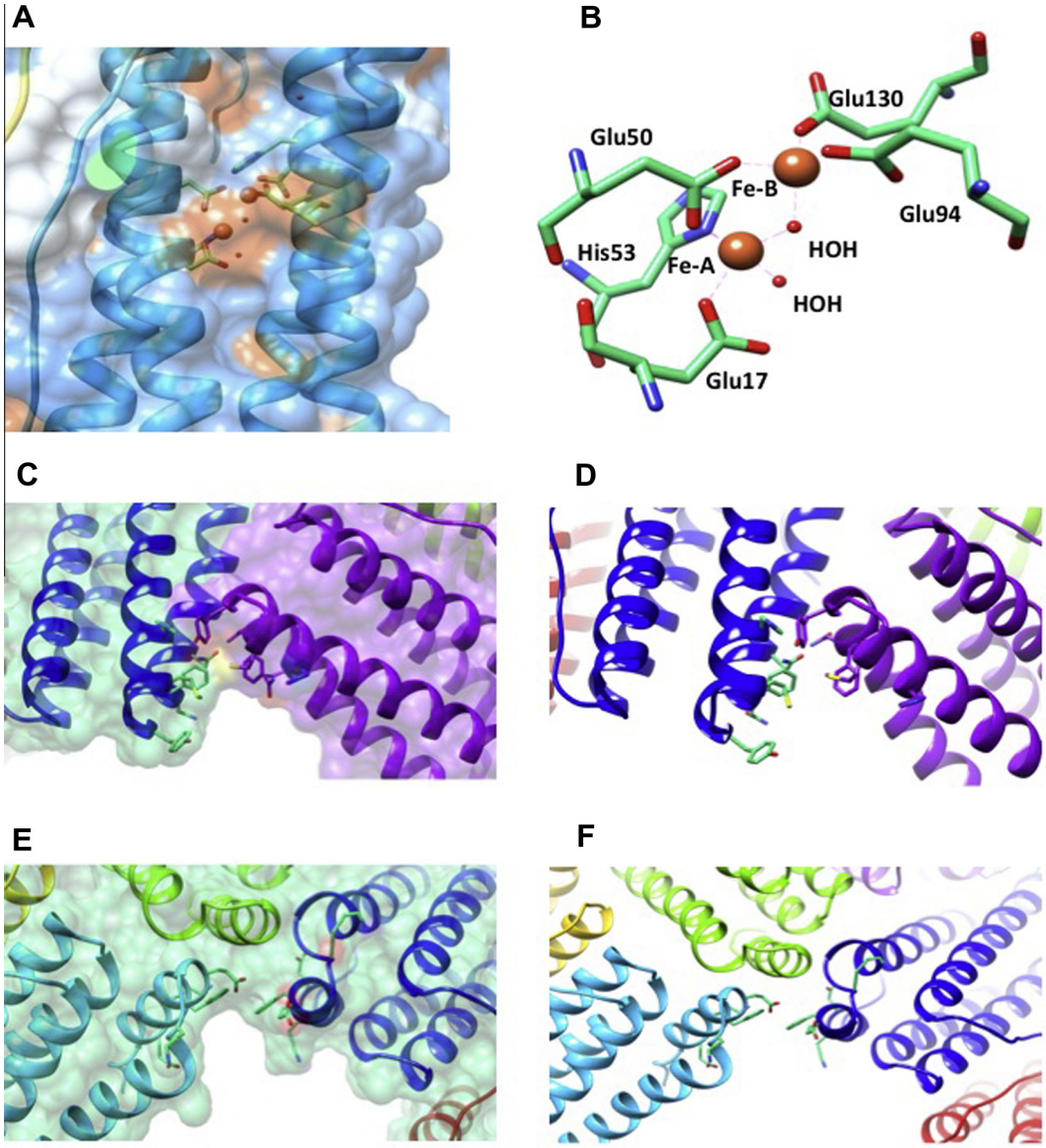

Fig. 2. The ferroxidase center, active site and pores of ferritin structures: (A) arrangement of ferroxidase center shows the surface representation, (B) the close-up view of the active site residue co-ordinated with Fe-ions, (C) surface view of 3-fold channels, (D) the residue which form the 3-fold channels are shown in stick model (His106, Tyr114, Asn118, Met109, Phe117 and Gln121), (E) surface representation of 4-fold channels and (F) the key residues for 4-fold channel formation are shown in the form of sticks (Lys146, Phe153, Glu157, Glu149 and Lys156).

3.2. Iron binding site

The electron density of binuclear iron site was observed in each monomer. In crystallized form, each monomer binds with two Fe atoms, in total twelve Fe atoms bind with hexameric structure. The Fe ion is bonded with Glu17, Glu50, Glu94, Glu130 and His53. Two Fe atoms are connected through the water molecule. The Fe–Fe distance was observed in the range of 3.3–3.5 Å and these were shown in Fig. 2A & B.

In our structure, the ferroxidase centers of A & B sites are binds with Fe ions. Whereas the (third) C site happened to be free, without any metal/ligand, confirmed from the electron density while refining the structure. The same binding mode was observed in Zn soaked structure in EcFtnA [7].

4. Discussion

The ferritin molecules control the iron storage and regulation (uptake and release) through pores present between the subunit structural organizations. The 3-fold and 4-fold channels are important for the iron entry/close mechanism. Through the pores iron atom easily travel to inner cavity of the molecules and stored as bio available form. Based on the starving conditions, the iron was released and utilized for its biological mechanism. The residues involving in the formation of channels are the gateway for the iron regulations. Existing research evidences suggested that the incorporation of metal ions are based on the presence of amino acids in the three/fourfold channels [20]. The three/fourfold channels are composed of His106, Tyr114, Asn118, Met109, Phe117 and Gln121/ Lys146, Phe153, Glu157, Glu149 and Lys156. The formation of pores and interaction residues are presented in both the channels are shown in Fig. 2 C–F.

Till date, the metal was incorporated in ferritin either from the added ferrous solution during crystallization or purification steps or soaking of crystals with the suitable metals (Fe, Zn, and Ca). In EcFtnA three types of structures were solved: (i) in apo-form, none of the metal ions were present in the A, B and C sites; (ii) when soaked with 10 mM ammonium ferrous sulfate for three hours,

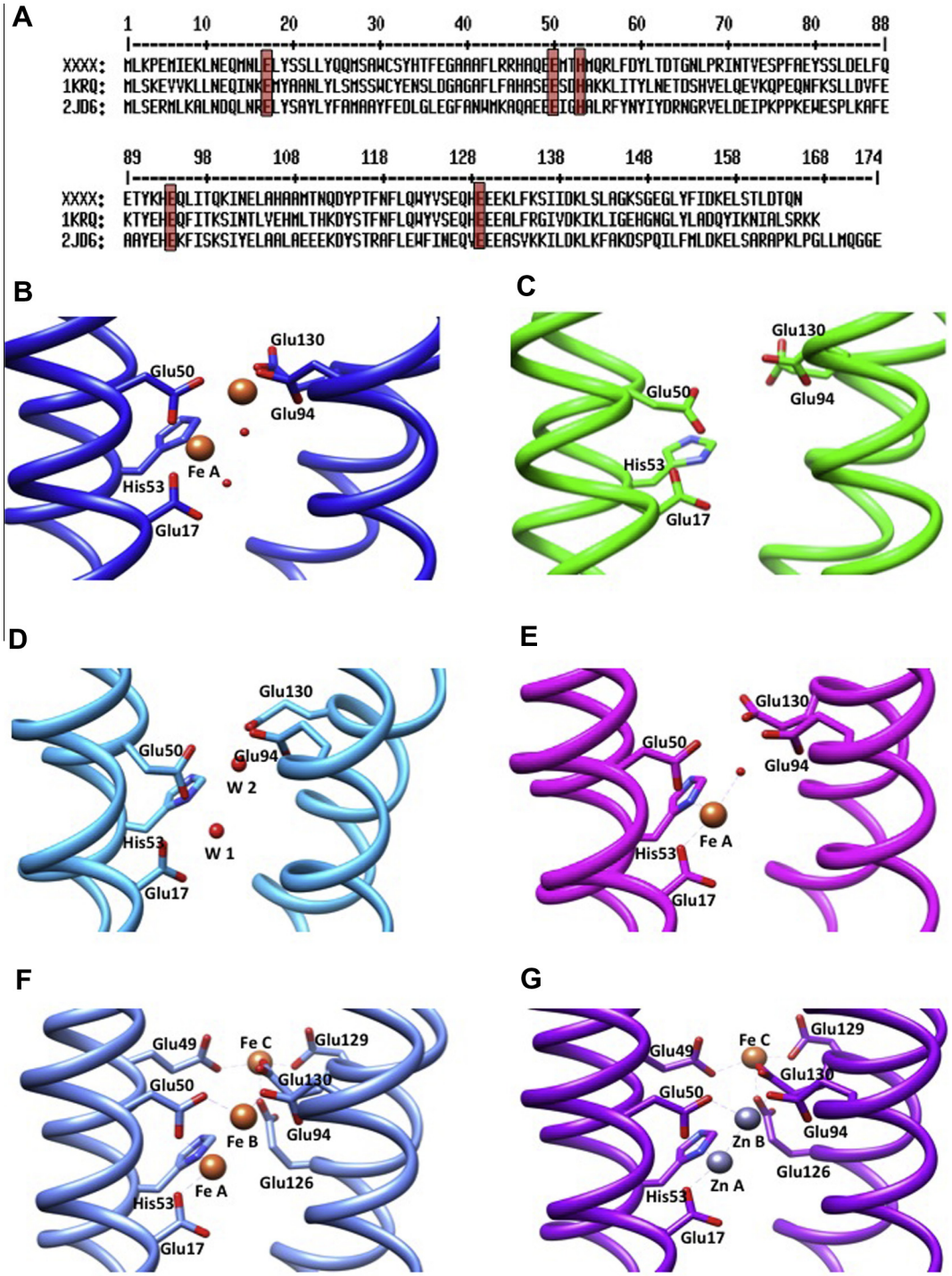

Fig. 3. Metal binding mechanism of ferritin was compared with other ferritin structures. (A) Sequence analysis of *E. coli* and related structures; the active site residues are shaded in brown color, (B) crystal structure of ferritin from *E. coli* (our structure) and its active site residue interactions with Fe-ions (A and B sites). The residues and Fe-ions are shown in ball-and-stick and gold spheres, respectively. (C) Reported apo form structure of ferritin from *E. coli* [PDB ID: 1EUM], (D) crystal structure of ferritin from *Campylobacter jejuni* [PDB ID: 1KRQ] shows the presence of two water molecules (represented in red spheres) at A and B sites. (E) The crystal structure of ferritin from *Pyrococcus furiosus* with Fe-ion at site A is shown with its active site residues [PDB ID: 2JD6], (F) crystal structure with three Fe-ions at the active sites A, B and C are shown as spheres [PDB ID: 2JD7], (G) the crystal structure represented in (F) with two Zn-ions at A and B sites and Fe ion at C were shown [PDB ID: 2JD8]. The protein residues and Fe-ions are represented as explained above and silver color spheres represent the Zn-ions. (For interpretation of the references to color in this figure legend, the reader is referred to the web version of this article.)

Fe ions were incorporated in all of the three (A, B and C) sites; and (iii) when soaked with 10 mM of Zinc Chloride, only the A and B sites were incorporated and not by C [7]. The ferritin structure derived from *Campylobacter jejuni* [PDB ID: 1KRQ] revealed that only two water molecules were present at A and B sites. When 20 mM of iron sulfate was mixed with ferritin from *Pyrococcus furiosus*, Fe ion binds at site A [PDB ID: 2JD6]. But when the crystal was soaked with 20 mM $FeSo_4$ solution for 15 min, all of the A, B & C sites were incorporated with Fe ions [PDB ID: 2JD7]. When the same procedure was repeated with $ZnSo_4$ for the period of 15 min, the A and B sites were replaced with Zn ions but site C was left out with Fe-ion [PDB ID: 2JD8] [20]. The metal binding

mechanism was compared with other structured and shown in Fig. 3A–G.

While modeling the crystal structure, we observed unambiguously two strong electron density peaks and those were fitted with $HgCl_2$ molecules and refined. These $HgCl_2$ molecules might have derived from heavy metal soaking solution, which we used prior to the data collection. Similarly, the modeled sulfate ions, Mg and MES molecules in the ferritin structure were also derived from the crystallization buffer.

In summary, the ferritin was expressed and purified. The purified protein was confirmed through N-terminal protein sequencing and MALDI-TOF spectroscopy. The protein was crystallized in I4 space group and data were collected in synchrotron source. The structure was solved by MR method. From the unambiguous electron density map, the endogenously bound binuclear iron sites were identified and discussed with the existing data.

Acknowledgments

We thank Ms. M. Okada for the experimental help. We also thank Dr. T. Ishikawa and Ms. Y. Matsumoto for moral support and encouragement. VT and MNP thank RIKEN SPring-8 Center for the RIKEN-Internship and Beam line access for data collection.

References

[1] P. Ponka, C. Beaumont, D.R. Richardson, Function and regulation of transferrin and ferritin, Semin. Hematol. 35 (1998) 35–54.
[2] D.M. Lawson, P.J. Artymiuk, S.J. Yewdall, J.M. Smith, J.C. Livingstone, A. Treffry, A. Luzzago, S. Levi, P. Arosio, G. Cesareni, et al., Solving the structure of human H ferritin by genetically engineering intermolecular crystal contacts, Nature 349 (1991) 541–544.
[3] L. Toussaint, L. Bertrand, L. Hue, R.R. Crichton, J.P. Declercq, High-resolution X-ray structures of human apoferritin H-chain mutants correlated with their activity and metal-binding sites, J. Mol. Biol. 365 (2007) 440–452.
[4] Y. Ha, D. Shi, G.W. Small, E.C. Theil, N.M. Allewell, Crystal structure of bullfrog M ferritin at 2.8 A resolution: analysis of subunit interactions and the binuclear metal center, J. Biol. Inorg. Chem. 4 (1999) 243–256.
[5] M.A. Michaux, A. Dautant, B. Gallois, T. Granier, B.L. d'Estaintot, G. Precigoux, Structural investigation of the complexation properties between horse spleen apoferritin and metalloporphyrins, Proteins 24 (1996) 314–321.
[6] T. Masuda, F. Goto, T. Yoshihara, B. Mikami, Crystal structure of plant ferritin reveals a novel metal binding site that functions as a transit site for metal transfer in ferritin, J. Biol. Chem. 285 (2010) 4049–4059.
[7] T.J. Stillman, P.D. Hempstead, P.J. Artymiuk, S.C. Andrews, A.J. Hudson, A. Treffry, J.R. Guest, P.M. Harrison, The high-resolution X-ray crystallographic structure of the ferritin (EcFtnA) of *Escherichia coli*; comparison with human H ferritin (HuHF) and the structures of the Fe(3+) and Zn(2+) derivatives, J. Mol. Biol. 307 (2001) 587–603.
[8] S.H. Banyard, D.K. Stammers, P.M. Harrison, Electron density map of apoferritin at 2.8-A resolution, Nature 271 (1978) 282–284.
[9] R.R. Crichton, Structure and function of ferritin, Angew. Chem. Int. Ed. Engl. 12 (1973) 57–65.
[10] P.M. Harrison, P. Arosio, The ferritins: molecular properties, iron storage function and cellular regulation, Biochim. Biophys. Acta 1275 (1996) 161–203.
[11] N.E. Le Brun, S.C. Andrews, J.R. Guest, P.M. Harrison, G.R. Moore, A.J. Thomson, Identification of the ferroxidase centre of *Escherichia coli* bacterioferritin, Biochem. J. 312 (Pt 2) (1995) 385–392.
[12] P. Rucker, F.M. Torti, S.V. Torti, Role of H and L subunits in mouse ferritin, J. Biol. Chem. 271 (1996) 33352–33357.
[13] L. Zhang, W. Sun, W. Cai, Z. Zhang, Y. Gu, H. Chen, S. Ma, X. Jia, Differential response of two ferritin subunit genes (VpFer1 and VpFer2) from *Venerupis philippinarum* following pathogen and heavy metals challenge, Fish Shellfish Immunol. (2013).
[14] K. Caban-Hernandez, J.F. Gaudier, A.M. Espino, Characterization and differential expression of a ferritin protein from *Fasciola hepatica*, Mol. Biochem. Parasitol. 182 (2012) 54–61.
[15] Z. Yang, X. Wang, H. Diao, J. Zhang, H. Li, H. Sun, Z. Guo, Encapsulation of platinum anticancer drugs by apoferritin, Chem. Commun. (Camb.) (2007) 3453–3455.
[16] R. Xing, X. Wang, C. Zhang, Y. Zhang, Q. Wang, Z. Yang, Z. Guo, Characterization and cellular uptake of platinum anticancer drugs encapsulated in apoferritin, J. Inorg. Biochem. 103 (2009) 1039–1044.
[17] B.W. Matthews, Solvent content of protein crystals, J. Mol. Biol. 33 (1968) 491–497.
[18] N. Collaborative, Computational Project, The CCP4 suite: programs for protein crystallography, Acta Crystallogr. D Biol. Crystallogr. 50 (1994) 760–763.
[19] P. Emsley, K. Cowtan, Coot: model-building tools for molecular graphics, Acta Crystallogr. D Biol. Crystallogr. 60 (2004) 2126–2132.
[20] J. Tatur, W.R. Hagen, P.M. Matias, Crystal structure of the ferritin from the hyperthermophilic archaeal anaerobe *Pyrococcus furiosus*, J. Biol. Inorg. Chem. 12 (2007) 615–630.